

Espaloma-0.3.0: Machine-learned molecular mechanics force field for the simulation of protein-ligand systems and beyond.

Kenichiro Takaba (ORCID: [0000-0002-2481-8830](https://orcid.org/0000-0002-2481-8830))^{1, 2}, Iván Pulido (ORCID: [0000-0002-7178-8136](https://orcid.org/0000-0002-7178-8136))¹,
Mike Henry (ORCID: [0000-0002-3870-9993](https://orcid.org/0000-0002-3870-9993))¹, Hugo MacDermott-Opeskin (ORCID: [0000-0002-7393-7457](https://orcid.org/0000-0002-7393-7457))¹,
John D. Chodera (ORCID: [0000-0003-0542-119X](https://orcid.org/0000-0003-0542-119X))¹,
Yuanqing Wang¹ (ORCID: [0000-0003-4403-2015](https://orcid.org/0000-0003-4403-2015))^{3, 1}

¹Computational and Systems Biology Program, Sloan Kettering Institute, Memorial Sloan Kettering Cancer Center, New York, N.Y. 10065; ²Pharmaceutical Research Center, Advanced Drug Discovery, Asahi Kasei Pharma Corporation, Shizuoka 410-2321, Japan; ³New York University, New York, N.Y. 10004

***For correspondence:**

john.chodera@choderlab.org (JDC); wangyq@wangyq.net (YW)

Abstract Molecular mechanics (MM) force fields—the models that characterize the energy landscape of molecular systems via simple pairwise and polynomial terms—have traditionally relied on human expert-curated, inflexible, and poorly extensible discrete chemical parameter assignment rules, namely atom or valence types. Recently, there has been significant interest in using graph neural networks to replace this process, while enabling the parametrization scheme to be learned in an end-to-end differentiable manner directly from quantum chemical calculations or condensed-phase data. In this paper, we extend the Espaloma [75] end-to-end differentiable force field construction approach by incorporating both energy and force fitting directly to quantum chemical data into the training process. Building on the OpenMM SPICE dataset [23], we curate a dataset containing chemical spaces highly relevant to the broad interest of biomolecular modeling, covering small molecules, proteins, and RNA. The resulting force field, `espaloma 0.3.0`, self-consistently parametrizes these diverse biomolecular species, accurately predicts quantum chemical energies and forces, and maintains stable quantum chemical energy-minimized geometries. Surprisingly, this simple approach produces highly accurate protein-ligand binding free energies when self-consistently parametrizing protein and ligand. This approach—capable of fitting new force fields to large quantum chemical datasets in one GPU-day—shows significant promise as a path forward for building systematically more accurate force fields that can be easily extended to new chemical domains of interest. The `espaloma 0.3.0` force field is available for use directly or within OpenMM via the open-source Espaloma package [<https://github.com/choderlab/espaloma>], and both the code and datasets for constructing this force field are openly available [<https://github.com/choderlab/refit-espaloma>].

Molecular mechanics force fields [15, 29] have long been a workhorse for biomolecular simulation and computer-aided drug design [45, 66]. These models—characterizing the conformational energetics and non-covalent interactions—have become instrumental to a wide variety of *in silico* biomolecular modeling tasks, including enumeration of putative bioactive conformations [14], hit identification via virtual screening [5],

¹Work partly done while at Memorial Sloan Kettering Cancer Center.

prediction of membrane permeability [71], simulations of biomolecular dynamics [61], and estimation of protein:ligand binding free energies via alchemical free energy calculations [54].

Traditional molecular mechanics force fields employ a set of rules termed *atom typing* to group atoms to share sets of parameters based on their elemental identity, hybridization, aromaticity, and number and properties of neighbors, subsequently assigning tabulated parameters based on the atom types composing the valence term [15, 29, 56]. This practice manifests several pathologies: Firstly, atoms of distinct chemical environments might share the same type and thereby parameters, leading to suboptimal *chemical resolution*; reducing errors requires the introduction of more fine-grained atom type descriptions, resulting in an explosion in the number of necessary atom types and parameter assignment table entries, especially for torsions [56]. Secondly, atom typing rules are traditionally constructed by human experts, whose design optimality cannot be quantitatively assessed; also, the evolution of such methodologies would constantly require engineer time and is not sustainable. Finally, discrepancies in these assignments might arise among different implementations in chemoinformatics toolkits [56].

More concerningly, biomolecular systems relevant to drug discovery are frequently highly heterogeneous. Atom type-based force fields are frequently developed separately for each class of biomolecules, enormously increasing the complexity of ensuring these force fields remain compatible, and risking poor accuracy when multiple classes of biomolecules must interact. As such, extension or expansion to new classes of biomolecules or chemical spaces becomes a time-consuming ordeal. For instance, the recent AmberTools 23 release [8] recommends combining independently developed force fields to simulate systems containing proteins [53], DNA [82], RNA [60], water [31], monovalent [36, 37] and divalent [47–49] counterions, lipids [28], carbohydrates [42], glycoconjugates [17, 18], small molecules [72, 73], post-translational modifications [38], and nucleic acid modifications [70].

Recently, Espaloma [75] (*extendable surrogate potential optimized by message-passing*) emerges as a novel approach to parametrize molecular mechanics (MM) force fields. Rather than relying on human experts, Espaloma (**Figure 1**) employs a graph neural network model (conditioned on neural network parameters Φ_{NN}) to construct continuous vectorial representations of atoms based on their chemical environments (Stage 1), combining them in a symmetry-preserving manner, to produce invariant latent-space representations of atom, bond, angle, and torsion chemical environments (Stage 2). These atom, bond, angle, and torsion representations can then be fed into neural modules to produce molecular mechanics parameters Φ_{FF} directly (Stage 3), rather than requiring lookup tables to assign parameters—enabling smooth interpolation between known chemical environments. Atomic partial charges can also be generated by this approach, with recent applications using a geometry-independent charge equilibration approach to rapidly generate AM1-BCC [33, 34] quality charges [74, 77]. This framework also enables rapid experimentation with new classes of molecular force fields, such as the addition of terms to represent point polarizability or higher-order couplings between valence terms in class II force fields [15, 29].

Constructing a complete force field with Espaloma is straightforward: Because the entire process of parameter assignment is end-to-end differentiable, the Espaloma neural network parameters (Φ_{NN}) can be optimized directly using a standard machine learning framework to fit quantum chemical and/or experimental data directly [75]. Operating on chemical graphs, Espaloma can rapidly and self-consistently generate parameters for any biomolecules with elemental coverage in its training set without the need to combine distinct force fields. Earlier work has demonstrated how both proteins and small molecules could rapidly and self-consistently be parameterized in under a second using a model jointly trained on a limited set of quantum chemical data covering small molecules and amino acids [75].

Here, we demonstrate how this approach can scale to foundational quantum chemical datasets that provide extensive coverage of heterogeneous biomolecular space. We present a new generation Espaloma model—`espaloma-0.3.0`—trained on a broad chemical space that includes small druglike molecules, peptides, nucleic acids, and fragments of a broad variety of biomolecular species. We fit both energies and forces from a rich quantum chemical dataset containing over 15,000 unique molecules and 1M conformations, which augment both the foundational SPICE quantum chemical dataset [23] and open quantum chemical datasets provided by the Open Force Field Initiative [63] hosted through QCArchive [68]. To ensure the model remains well-behaved when trained on very large datasets, we fine-tune Espaloma’s loss

function to incorporate significantly more regularization to enhance its stability. With extensive testing and benchmarking, we show that `espaloma-0.3.0` is highly capable in popular MD modeling tasks, including modeling protein-ligand binding.

The main contributions of this paper are summarized as follows:

- Chemically and conformationally diverse datasets of interest to biomolecular modeling are curated to enable the construction of molecular mechanics (MM) force fields that can be applied to small molecules, proteins, RNA, and beyond.
- A training strategy that uses both energies and forces along with regularization is developed to enable Espaloma to parametrize force fields that demonstrate robustness and good agreement with quantum chemical energy surfaces.
- The newly constructed force field, `espaloma-0.3.0`, produces not only accurate quantum conformational energetics, but also accurate protein-ligand binding free energy estimates vis-à-vis experimental data; this holds true for when `espaloma-0.3.0` is used to parametrize both protein and small molecule, or just the small molecule (when combined with a protein force field `espaloma-0.3.0` is designed to be compatible with). The accuracy and correlation are on par with popular legacy force fields produced by decades of expert-guided work.

1 Espaloma provides a flexible, end-to-end differentiable framework for assigning molecular mechanics (MM) parameters using graph neural networks (GNNs)

Espaloma [75] (**Figure 1**) operates analogously to a legacy force field typing scheme to generate molecular mechanics (MM) force field parameters Φ_{FF} from a molecular graph \mathcal{G} and graph neural network (NN) parametrized by neural model parameters Φ_{NN} ,

$$\Phi_{FF} \leftarrow \text{espaloma}(\mathcal{G}, \Phi_{NN}). \quad (1)$$

The resulting parameters Φ_{FF} can then be subsequently used in a standard molecular mechanics package to compute the MM energy and forces for any conformation, as with a standard MM force field.

Espaloma parametrizes molecular systems in three sequential stages (**Figure 1**):

Stage 1: Graph neural networks generate a continuous vectorial atom embedding, replacing legacy discrete atom typing. First, using chemoinformatics toolkits such as RDKit [64], the molecular system is abstracted as a *graph*, with nodes denoting atoms and edges covalent bonds. Espaloma uses graph neural networks [3, 21, 22, 26, 41, 74, 76, 78, 79, 81] as a replacement for rule-based chemical environment perception [56] to operate on this graph. These neural architectures learn useful representations of atomic chemical environments from simple input features by updating and pooling embedding vectors via message-passing iterations to neighboring atoms [26]. As such, symmetries in chemical graphs (chemical equivalencies) are inherently preserved, while a rich, continuous, and differentiably learnable representation of the atomic environment is derived.

Stage 2: Symmetry-preserving pooling generates continuous bond, angle, and torsion embeddings, replacing discrete types. The representations determined by GNNs in Stage 1 are used to come up with bond, angle, and torsion representations in a symmetry-preserving manner, where the relevant equivalent atom permutations are listed and summed up via Janossy pooling [57].

Stage 3: Neural parametrization of atoms, bonds, angles, and torsions replaces tabulated parameter assignment. In the final stage, feed-forward neural networks learn the mapping from these symmetry-preserving invariant atom, bond, angle, and torsion encodings to MM parameters Φ_{FF} that reflect the specific chemical environments appropriate for these terms. Each distinct parameter class (such as atom parameters, bond parameters, angle parameters, and torsion parameters) is assigned by a separate neural network, making this stage fully modular. This stage is analogous to the final table lookup step in traditional force field construction but with significant added flexibility arising from the continuous embedding that captures the chemical environment specific to the potential energy term being assigned. The

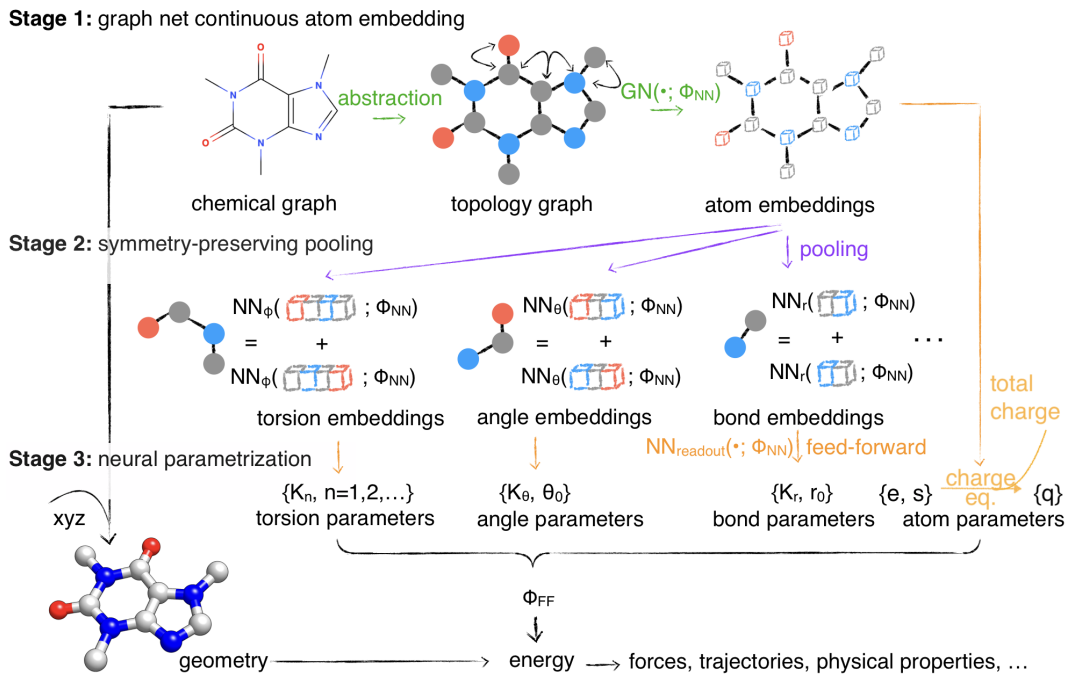


Figure 1. Espaloma is an end-to-end differentiable molecular mechanics parameter assignment scheme for arbitrary organic molecules. espaloma (*extendable surrogate potential optimized by message-passing*) is a modular approach for directly computing molecular mechanics force field parameters Φ_{FF} from a chemical graph G such as a small molecule or biopolymer via a process that is fully differentiable in the model parameters Φ_{NN} . In **Stage 1**, a graph neural network is used to generate continuous latent atom embeddings describing local chemical environments from the chemical graph. In **Stage 2**, these atom embeddings are transformed into feature vectors that preserve appropriate symmetries for atom, bond, angle, and proper/improper torsion inference via Janossy pooling [57]. In **Stage 3**, molecular mechanics parameters are directly predicted from these feature vectors using feed-forward neural nets. This parameter assignment process is performed once per molecular species, allowing the potential energy to be rapidly computed using standard molecular mechanics or molecular dynamics frameworks thereafter. The collection of parameters Φ_{NN} describing the espaloma model can be considered as the equivalent complete specification of a traditional molecular mechanics force field such as GAFF [72, 73]/AM1-BCC [33, 34] in that it encodes the equivalent of traditional typing rules, parameter assignment tables, and even partial charge models. Figure reproduced from the arXiv preprint of Wang et al. [75] under license <http://arxiv.org/licenses/nonexclusive-distrib/1.0/>.

output of Stage 3, and the entire pipeline, is a set of force field parameters Φ_{FF} uniquely determined by the neural network conditioned on its associated weights Φ_{NN} .

Overall, the Espaloma framework is end-to-end differentiable—the error in energy (or the function thereof, such as forces) can be backpropagated to optimize the force field parameters Φ_{FF} , and thereby neural network parameters Φ_{NN} that govern how they are produced from the input molecule. Stage 3 is especially modular and flexible: New force field terms that act on atoms, bonds, angles, torsions, or combinations thereof can easily be added and the entire force field refit starting from either an existing Φ_{NN} or training from scratch. In this way, Espaloma provides a rapid and flexible approach to experimenting with different potential functions (such as the addition of point polarizability or exploration of alternative functional forms) or retraining with augmented training datasets.

2 An extensive quantum chemical dataset was curated to provide coverage of small molecules, proteins, nucleic acids, and other biomolecules

While the initial Espaloma model described in Wang et al. [75] had extremely limited chemical space coverage, it demonstrated the potential to provide self-consistent coverage of multiple classes of biomolecules. In Wang et al. [75], the quantum chemical training set was limited to 792 small molecules and 1528 di- and tri-peptides, providing a useful proof of concept that was competitive with other noncommercial small

molecule and protein force fields, but far from providing comprehensive coverage of chemical space relevant to drug discovery and biomolecular modeling.

To demonstrate that Espaloma can scale to provide high-quality coverage on large regions of biomolecular space when systematically parameterized on a large quantum chemical dataset, we constructed a significantly expanded dataset with the intention of producing a force field that was broadly applicable to biomolecular modeling and computer-aided drug discovery (**Table 1**). This quantum chemical dataset is built from several components that provide complementary coverage of relevant biomolecular chemistries: From the foundational SPICE dataset [23], we extracted a large set of druglike small molecules selected from PubChem [50], dipeptides and their common protonation and tautomeric variants, and diverse molecular fragments providing broad coverage of biomolecules from the DES370K dataset [19]; from the OpenFF 1.x ("Parsley") [63] and 2.x ("Sage") [7] datasets, we extracted optimization and torsion-drive datasets for diverse small molecules; a diverse set of dipeptide, tripeptides, disulfide-bridged, bioactive, and cyclic peptides from the PepConf dataset [62]; a peptide torsion scan set generated by the Open Force Field Consortium for the OpenFF 3.x ("Rosemary") force field [9]; and a new set of RNA nucleosides, trinucleotides, and diverse experimental RNA fragments from the Nucleic Acid Database [13] and RNA Structure Atlas [58] to extend coverage to this important and growing class of drug targets. Complete details of the dataset construction and composition are given in **SI Section B**.

All quantum chemical energies were computed with the Open Force Field (OpenFF) standard level of quantum chemical theory (B3LYP-D3BJ/DZVP) [7, 63], generated with the open source psi4 quantum chemistry package [69] using the QCArchive [68] QCFractal infrastructure via OpenFF QCSubmit [32] workflows. The final dataset used to construct and assess the `espaloma-0.3.0` model contains 17,427 unique molecules and 1,188,317 conformations in total. This dataset is publicly available for download (see **SI Section B**).

Dataset Name	Category	Mols	Confs	Split	espaloma-0.3.0		Baseline Force Field (Test molecules)					
					Energy RMSE (kcal/mol)		Energy RMSE (kcal/mol)					
					Force RMSE (kcal/mol · Å ⁻¹)		Force RMSE (kcal/mol · Å ⁻¹)					
					Train (80%)	Test (10%)	gaff-2.11	openff-2.0.0	openff-2.1.0	ff14SB/RNA.O13		
SPICE-Pubchem [23, 39] (Dataset)	Small molecule	14110	608436	80:10:10	2.21 ^{2.22} _{2.20}	2.52 ^{2.56} _{2.48}	4.64 ^{4.69} _{4.60}	4.43 ^{4.47} _{4.38}	4.71 ^{4.75} _{4.66}			
					6.18 ^{6.18} _{6.17}	6.87 ^{6.89} _{6.85}	14.38 ^{14.40} _{13.35}	13.94 ^{13.96} _{13.92}	15.53 ^{15.56} _{15.51}			
SPICE-DES-Monomers [20, 23] (Dataset)	Small molecule	369	18435	80:10:10	1.50 ^{1.53} _{1.46}	1.68 ^{1.80} _{1.56}	2.12 ^{2.30} _{1.97}	2.63 ^{2.44} _{2.41}	2.71 ^{2.95} _{2.50}			
					5.94 ^{5.97} _{5.91}	6.05 ^{6.14} _{5.97}	10.74 ^{10.88} _{10.61}	12.07 ^{12.21} _{11.94}	12.59 ^{12.71} _{12.46}			
Gen2-Opt [1] (OptimizationDataset)	Small molecule	1024	244989	80:10:10	1.66 ^{1.70} _{1.63}	2.05 ^{2.18} _{1.95}	3.36 ^{3.46} _{3.28}	2.68 ^{2.86} _{2.59}	2.77 ^{2.86} _{2.69}			
					3.65 ^{3.67} _{3.64}	4.53 ^{4.58} _{4.49}	10.94 ^{10.96} _{10.91}	10.97 ^{11.00} _{10.95}	11.31 ^{11.33} _{11.28}			
Gen2-Torsion [1] (TorsionDriveDataset)	Small molecule	729	25832	80:10:10	2.71 ^{2.76} _{2.66}	2.40 ^{2.46} _{2.34}	2.94 ^{2.05} _{2.85}	2.49 ^{2.55} _{2.44}	2.77 ^{2.84} _{2.70}			
					4.26 ^{4.28} _{4.24}	4.35 ^{4.37} _{4.33}	10.37 ^{10.41} _{10.32}	10.75 ^{10.80} _{10.71}	10.62 ^{10.66} _{10.58}			
SPICE-Dipeptide [23] (Dataset)	Peptide	677	26279	80:10:10	3.27 ^{3.30} _{3.23}	3.15 ^{3.25} _{3.05}	4.28 ^{4.42} _{4.15}	4.15 ^{4.29} _{4.14}	4.35 ^{4.50} _{4.22}	4.44 ^{4.57} _{4.29}		
					7.99 ^{7.99} _{7.97}	7.85 ^{7.90} _{7.80}	11.98 ^{12.05} _{11.92}	12.01 ^{12.06} _{11.95}	11.61 ^{11.66} _{11.56}	11.82 ^{11.88} _{11.77}		
Pepconf-Opt [2, 62] (OptimizationDataset)	Peptide	557	166291	80:10:10	2.78 ^{2.84} _{2.73}	3.09 ^{3.27} _{2.95}	5.16 ^{5.27} _{5.05}	4.32 ^{4.48} _{4.19}	4.62 ^{4.75} _{4.50}	4.38 ^{4.49} _{4.28}		
					3.50 ^{3.51} _{3.48}	3.76 ^{3.81} _{3.57}	10.15 ^{10.17} _{10.12}	9.61 ^{9.63} _{9.58}	9.79 ^{9.81} _{9.77}	10.13 ^{10.15} _{10.11}		
Protein-Torsion (TorsionDriveDataset)	Peptide	62	48999	80:10:10	2.51 ^{2.55} _{2.47}	2.08 ^{2.14} _{2.01}	3.22 ^{3.35} _{3.08}	2.97 ^{3.10} _{2.85}	3.37 ^{3.54} _{3.22}	3.19 ^{3.31} _{3.06}		
					4.08 ^{4.10} _{4.06}	3.62 ^{3.67} _{3.57}	8.01 ^{8.05} _{7.97}	8.77 ^{8.81} _{8.73}	9.02 ^{9.06} _{8.98}	9.29 ^{9.32} _{9.24}		
RNA-Diverse (Dataset)	RNA	64	3703	80:10:10	4.22 ^{4.37} _{4.08}	4.06 ^{4.40} _{3.69}	5.72 ^{5.23} _{5.27}	5.76 ^{6.23} _{5.79}	6.44 ^{6.99} _{5.97}	5.97 ^{6.44} _{5.54}		
					4.41 ^{4.42} _{4.40}	4.35 ^{4.38} _{4.32}	16.94 ^{16.06} _{16.92}	18.19 ^{18.38} _{18.02}	19.69 ^{19.84} _{19.51}	19.15 ^{19.33} _{18.97}		
RNA-Trinucleotide (Dataset)	RNA	64	35811	0:0:100	3.86 ^{3.96} _{3.77}	5.93 ^{5.99} _{5.88}	4.24 ^{4.25} _{4.23}	17.09 ^{17.10} _{17.08}	18.70 ^{18.72} _{18.68}	20.02 ^{20.04} _{20.01}	19.70 ^{19.72} _{19.69}	
RNA-Nucleoside (Dataset)	RNA	4	9542	100:0:0	1.33 ^{1.39} _{1.28}	4.17 ^{4.18} _{4.15}	2.72 ^{2.77} _{2.67}	2.30 ^{2.34} _{2.26}	2.00 ^{2.03} _{1.97}	2.48 ^{2.51} _{2.44}		
								13.80 ^{13.84} _{13.77}	14.02 ^{14.05} _{13.99}	15.41 ^{15.45} _{15.38}	14.18 ^{14.21} _{14.14}	

Table 1. espaloma-0.3.0 can directly fit quantum chemical potential energies and forces more accurately than the baseline force fields. Espaloma was fit to quantum chemical potential energies and forces from various QM datasets sourced from QCArchive [68], covering a broad chemical space that includes small molecules, peptides, and RNA molecules (see **SI Section B**). The entire dataset consists of 17,427 unique molecules and 1,188,317 conformations. These datasets were extracted from three different QCArchive workflows: BasicDataset, OptimizationDataset, and TorsionDriveDataset. Except for RNA-Trinucleotide and RNA-nucleoside dataset, all datasets were partitioned into train, validate, and test sets in an 80:10:10 ratio based on molecules. Due to the lack of chemically diversity, only the RNA-diverse dataset was partitioned similarly to the other datasets, whereas the entire RNA-nucleoside dataset was considered during training while the RNA-trinucleotide dataset was used solely for the test set. The number of molecules and total conformations for each dataset is annotated in the table. We report the root mean square error (RMSE) on the training and test sets, along with the performance of other force fields as baselines on the test set. Note that the reported baseline force field RMSE for RNA-Nucleoside uses the same train dataset to report espaloma-0.3.0 RMSE. All statistics are computed with predicted and reference energies centered to have a zero mean for each molecule similar to the previous work [75]. The 95% confidence intervals, annotated in the results, were calculated by bootstrapping molecular conformers with replacement using 1000 replicates.

3 `espaloma-0.3.0` accurately predicts quantum chemical energies and forces

Leveraging the datasets generated in Section 2, we refit the Espaloma force field. Similar to the original implementation, since the van der Waals parameters affect the physical property prediction, which is computationally challenging to optimize, we only optimize the valence parameters while using `openff-2.0.0` [6]—we leave the tuning of van der Waals parameters for future study. For partial charges, following the protocol of Wang et al. [76], we predict the electronegativity and hardness of atoms before using *charge equilibration* [27] to predict atomic partial charges while preserving the total charge exactly. We improve the training pipeline of the original Espaloma force field to increase its stability and data efficiency:

- Quantum mechanics forces are incorporated into training.
- Strong $L2$ regularization is applied on proper and improper torsion force constants.
- We truncate the improper torsion terms to include only $n = 1, 2$ periodicities.

To generate the `espaloma-0.3.0` force field, we randomly shuffle the datasets and split each into train, test, and validation sets (80%, 10%, and 10%, respectively) based on chemical species (unique isomeric SMILES strings). Since the MM force field is incapable of reproducing quantum chemical heats of formation, which are reflected as an additive offset in quantum chemical energy targets, we shift the reference energy to have zero mean; note that when deployed, the absolute value of MM energy is not physically meaningful and traditional MM force fields are never used to simulate bond-breaking events.

As shown in Table 1, `espaloma-0.3.0` significantly outperforms all baseline force fields in predicting QM energies and forces, demonstrating the ability of `espaloma-0.3.0` to recapitulate the QM energy landscape, while legacy force fields widely popular in the field of MD modeling yield considerable energy errors and huge force errors (on average twice to thrice of that of `espaloma-0.3.0`) vis-à-vis QM calculations. The performance superiority holds true across diverse chemical landscapes (as discussed in Section 2)—small molecules and biopolymers and conformational landscape—MD trajectories, optimization trajectories, and torsion scans, suggesting general utility of `espaloma-0.3.0` in a wide array of chemical and biochemical modeling tasks, as evidenced in Section 5.

4 `espaloma-0.3.0` preserves quantum mechanics energy minima

We examined whether the `espaloma-0.3.0` force field described in Section 3 not only quantitatively reproduced quantum chemical equilibrium conformational energetics, but was able to also qualitatively preserve quantum chemical local minima. To assess this, we initiated MM energy minimizations from QM-optimized conformations from the FDA Optimization Dataset in QCArchive [32]. Specifically, we selected the minimum quantum chemical energy snapshot for each molecule in the dataset and minimized with `espaloma`-derived force field, `openff-2.0.0` [6], `openff-2.1.0` [4], and `gaff-2.11` MM force fields using an L-BFGS optimizer with a 0.1 kJ/mol convergence tolerance. Figure 2 shows a kernel density estimate (KDE, upper) and an empirical cumulative density function (CDF, lower) of the aligned rooted mean square distance (RMSD) from the quantum chemical minimum produced by each force field. We noticed that `espaloma-0.3.0` preserves quantum mechanics energy minima better (“not optimized away”) compared to legacy force fields.

5 `espaloma-0.3.0` supports accurate alchemical free energy calculations.

To assess whether the small molecule parameters and charges generated by `espaloma-0.3.0` achieves competitive performance with a well-established force field, `openff-2.1.0` [4], we used the `perses 0.10.1` relative alchemical free energy calculation infrastructure [65] to compare the performance on a curated protein-ligand benchmark dataset. We work with four well-studied protein-ligand binding systems:

- Tyk2 (PDB: `4GIH`) [51], a non-receptor tyrosine-protine kinase, has therapeutic significance in inflammatory bowel diseases (IBD); this particularly popular system has good convergence;
- Cdk2 (PDB: `1H1Q`) [16], a cyclin-dependent kinase, is involved in molecular pathology of cancer and is, therefore, a popular target for structure-based drug design; we use this system, complex with cyclin A, to test the capability of parametrizing multiple protein subunits;

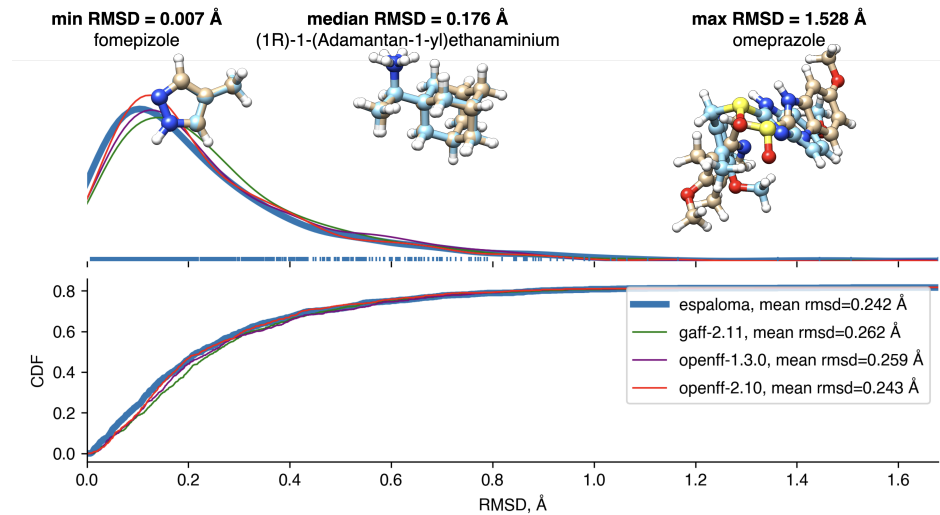


Figure 2. Espaloma-derived molecular mechanics force fields preserve the location of quantum chemical minima. Kernel density estimate (KDE) plot (upper) and empirical cumulative density function (CDF) of aligned root mean square deviation (RMSD) between quantum chemical minima and MM-optimized minima using parameters from either espaloma-generated molecular mechanics or legacy force fields. This qualitative experiment shows that the energy minima determined by espaloma-0.3.0 is close to the QM minima.

ff14SB+openff-2.1.0											
System	PDB ID	Compds	Edges	$\Delta\Delta G$ (kcal/mol)	ns/replica	Relative		Absolute			
						RMSE	MUE	RMSE	MUE	R^2	Spearman ρ
Tyk2	4GIH	13	12	3.47	10	0.54 ^{0.71} _{0.36}	0.45 ^{0.62} _{0.28}	0.50 ^{0.64} _{0.36}	0.42 ^{0.57} _{0.27}	0.80 ^{0.93} _{0.53}	0.89 ^{0.96} _{0.75}
Cdk2	1H1Q	10	9	2.78	10	1.43 ^{1.75} _{1.04}	1.29 ^{1.67} _{0.80}	0.74 ^{0.93} _{0.50}	0.63 ^{0.86} _{0.41}	0.48 ^{0.85} _{0.13}	0.69 ^{0.92} _{0.30}
Mcl1	4HW3	25	24	4.19	15	1.50 ^{2.12} _{0.83}	1.02 ^{1.55} _{0.63}	1.36 ^{2.01} _{0.77}	0.97 ^{1.41} _{0.66}	0.50 ^{0.73} _{0.35}	0.71 ^{0.86} _{0.57}
P38	3FLY	28	27	3.81	20	1.06 ^{1.30} _{0.81}	0.87 ^{1.09} _{0.65}	0.90 ^{1.19} _{0.60}	0.69 ^{0.92} _{0.50}	0.57 ^{0.78} _{0.38}	0.76 ^{0.89} _{0.63}

ff14SB+espaloma-0.3.0											
System	PDB ID	Compds	Edges	$\Delta\Delta G$ (kcal/mol)	ns/replica	Relative		Absolute			
						RMSE	MUE	RMSE	MUE	R^2	Spearman ρ
Tyk2	4GIH	13	12	3.47	10	0.70 ^{0.98} _{0.34}	0.52 ^{0.80} _{0.28}	0.48 ^{0.65} _{0.29}	0.37 ^{0.55} _{0.23}	0.79 ^{0.95} _{0.49}	0.89 ^{0.97} _{0.71}
Cdk2	1H1Q	10	9	2.78	10	1.15 ^{1.44} _{0.85}	1.05 ^{1.36} _{0.73}	0.56 ^{0.74} _{0.32}	0.46 ^{0.66} _{0.27}	0.63 ^{0.92} _{0.27}	0.80 ^{0.96} _{0.53}
Mcl1	4HW3	25	24	4.19	15	1.38 ^{1.96} _{0.90}	1.06 ^{1.44} _{0.76}	1.51 ^{2.15} _{0.90}	1.08 ^{1.56} _{0.74}	0.60 ^{0.80} _{0.42}	0.77 ^{0.90} _{0.63}
P38	3FLY	28	27	3.81	20	1.03 ^{1.26} _{0.81}	0.82 ^{1.05} _{0.59}	1.10 ^{1.32} _{0.86}	0.88 ^{1.13} _{0.63}	0.38 ^{0.64} _{0.11}	0.62 ^{0.80} _{0.34}

espaloma-0.3.0											
System	PDB ID	Compds	Edges	$\Delta\Delta G$ (kcal/mol)	ns/replica	Relative		Absolute			
						RMSE	MUE	RMSE	MUE	R^2	Spearman ρ
Tyk2	4GIH	13	12	3.47	10	0.67 ^{0.87} _{0.45}	0.56 ^{0.76} _{0.35}	0.46 ^{0.58} _{0.33}	0.40 ^{0.53} _{0.28}	0.81 ^{0.94} _{0.64}	0.90 ^{0.97} _{0.79}
Cdk2	1H1Q	10	9	2.78	10	0.84 ^{1.05} _{0.58}	0.75 ^{0.99} _{0.51}	0.63 ^{0.76} _{0.48}	0.58 ^{0.74} _{0.41}	0.47 ^{0.82} _{0.14}	0.68 ^{0.90} _{0.41}
Mcl1	4HW3	25	24	4.19	15	1.44 ^{1.99} _{0.96}	1.10 ^{1.50} _{0.76}	1.40 ^{2.09} _{0.78}	1.00 ^{1.43} _{0.67}	0.56 ^{0.78} _{0.40}	0.75 ^{0.88} _{0.63}
P38	3FLY	28	27	3.81	20	1.02 ^{1.24} _{0.77}	0.79 ^{1.04} _{0.56}	0.91 ^{1.13} _{0.68}	0.75 ^{0.95} _{0.57}	0.47 ^{0.68} _{0.24}	0.68 ^{0.82} _{0.49}

Table 2. Protein-ligand alchemical free energy calculation benchmarks show espaloma-0.3.0 achieves high accuracy that is competitive to well-established force fields. Here, we report several different metrics to assess the performance of the protein-ligand binding benchmark results including root mean square error (RMSE), mean unsigned error (MUE), the square of the correlation coefficient (R^2), and the Spearman's rank correlation coefficient (ρ) along with 95% CI for each metric. The initial PDB ID, number of compounds, number of edges, the binding affinity range ($\Delta\Delta G$), and the simulation time per replica are reported in the table.

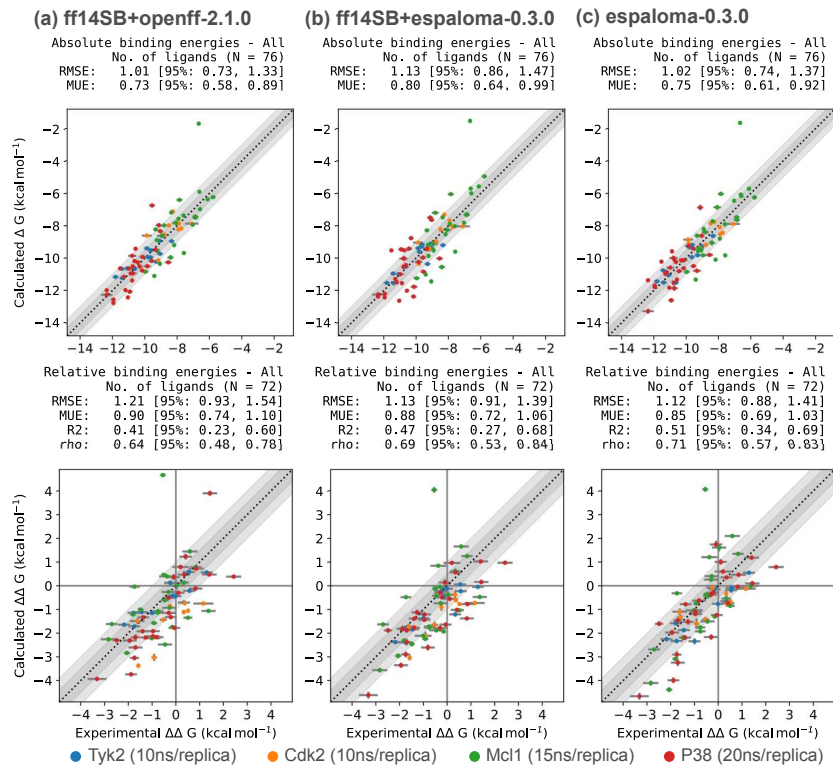


Figure 3. espaloma-0.3.0 can be used for accurate protein-ligand alchemical free energy calculations. Protein-ligand (PL) alchemical free energy calculations were calculated for TYK2 (10 ns), CDK2 (10 ns), MCL1 (15 ns), P38 (20 ns) using a curated PL-benchmark dataset which comprises 76 ligands in total. Here, we used Perses 0.10.1 relative free energy calculation infrastructure [65], based on OpenMM 8.0.0 [24], to assess the accuracy of espaloma-0.3.0 and openff-2.1.0 for comparison. (a) The openff-2.1.0 with protein parametrized with Amber ff14SB force field [53] achieves an absolute free energy (ΔG) RMSE of 1.01 [95% CI: 0.73, 1.33] kcal/mol. (b) The espaloma-0.3.0 for predicting valence parameters and partial charges of small molecules combined with Amber ff14SB force field for proteins achieves an absolute free energy (ΔG) RMSE of 1.13 [95% CI: 0.86, 1.47] kcal/mol. (c) Parametrizing small molecule and protein self-consistently with espaloma-0.3.0 achieves absolute free energy (ΔG) RMSE of 1.02 [95% CI: 0.74, 1.37] kcal/mol which is comparable to those obtained by (a) and (b). All systems were solvated with TIP3P water and neutralized with 300 mM NaCl salt using Jorg and Cheatham monovalent counterions. The light and dark gray regions depict the -0.5 kcal/mol and 1.0 kcal/mol confidence bounds.

- P38 (PDB: 3FLY) [43] is a mitogen-activated protein (MAP) kinase which is a central component in signaling networks in mammalian cell types; this target is another well-studied system, but is expected to be more challenging compared to Tyk2 and Cdk2 because of the larger ligand transformations and exploration of structure-activity relationships with multiple R-groups from different scaffold positions;
- Mcl1 (PDB: 4HW3) [25] (myeloid cell leukemia 1) is a member of the Bcl-2 family of proteins, is overexpressed in various cancers and promotes aberrant survival of tumor cells; this target entails all ligands with a net charge of -1 and includes scaffold hopping, thus chosen to test the capability of simulating free energy calculations for charged ligands and scaffold hopping;

These target systems have been adopted from Open Force Field [11] protein-ligand benchmark where the protein structures and ligand poses, as well as the ligand transformation networks were manually curated (see **SI Section D**). Within each system, we benchmark two approaches of parametrization:

- **Ligand-only.** We first apply espaloma-0.3.0 to only the *ligand* region of a protein-ligand system, to provide head-to-head comparison with a well-established small molecule force field openff-2.1.0 [4]; the protein parameters were assigned by Amber ff14SB force field [53].
- **Protein-ligand self-consistently.** We apply espaloma-0.3.0 to both the *ligand* as well as the *protein* region of the system; this is to test the capability of espaloma-0.3.0 to entirely replace the force field

parametrization pipeline.

All systems were solvated with TIP3P water [35] and neutralized with the Joung and Cheatham monovalent counterions [36].

In Figure 3 and Table 2, we illustrate that `espaloma-0.3.0` has *comparable* protein-ligand binding free energy performance with the combination of Amber ff14SB [53] and `openff-2.1.0` [4] force fields—the reported error and correlation statistics have overlapping confidence interval. In almost all cases, the performance of using `espaloma-0.3.0` on both the protein and ligand system are slightly higher than using `espaloma-0.3.0` on ligand only and resorting to Amber ff14SB [53] for protein parametrization.

We also compared the protein-ligand binding free energy calculations using the first generation `espaloma` model, `espaloma-0.2.2` [75], which was trained on a limited quantum chemical dataset compared to `espaloma-0.3.0`. The system was prepared similarly to those described above. In SI Figure 4, `espaloma-0.2.2` significantly underperforms compared to `espaloma-0.3.0` for the Cdk2 system due a large outlier. `espaloma-0.2.2` also demonstrates lesser performance on the Tyk2 system, as illustrated in SI Figure 5. Importantly, the protein-ligand binding free energy calculations were unstable for Mcl1 and P38, with many of the ligand transformations being suspended during the simulation. These results indicate that `espaloma-0.3.0`, trained on an extensive quantum chemical dataset and with an improved training strategy, has resulted in the development of a superior `espaloma` model.

6 Conclusion

Here, we demonstrate that the new `espaloma-0.3.0` force field can capture the quantitative and qualitative behavior of quantum mechanics on a wide variety of chemical landscapes. As a result, it produces accurate absolute and relative binding free energies estimates. We hope this work will lay the foundations to inspire the design of new generations of machine learning-empowered molecular mechanics force fields.

6.1 Chemically and conformationally diverse quantum chemical datasets curated to construct biomolecular MM force fields

Though Wang et al. [75] laid the foundation of machine learning molecular mechanics (MM) force field construction, the example force field released with its implementation is demonstrative rather than impactful because of the limited diversity it was trained on. In this paper, we tackle this problem squarely by assembling a high-quality dataset covering chemical spaces and conformational regions of interest to biomolecular simulation. We release this dataset with our implementation in the hope that this will encourage the community to further optimize MM force fields.

6.2 `espaloma-0.3.0` recapitulates the energy landscape of quantum mechanics

It has been shown, in this paper in Table 1 and previously [11] that legacy force fields typically have considerable disagreement with quantum mechanics (QM) calculations in terms of the force and energy predictions. With carefully crafted training and regularization strategies, we show that `espaloma-0.3.0` is much closer to the QM energy landscapes and *qualitatively* behave similarly to QM as well.

6.3 `espaloma-0.3.0` accurately predicts protein-ligand binding free energy with further improvement possible via direct optimization with regard to experimental free energy

The field of computational chemistry has relied on decades-old force fields (with limited continuous evolution) for MD simulation and free energy calculations. In this paper, we show, by merely fitting quantum mechanics data, we can curate a force field just as powerful in a few GPU hours, as opposed to countless engineer years. For future study, we plan to further optimize force fields under the Espaloma framework directly incorporating experimental binding free energy targets.

7 Disclosures

J.D.C. is a current member of the Scientific Advisory Board of OpenEye Scientific Software, Redesign Science, Ventus Therapeutics, and Interline Therapeutics, and has equity interests in Redesign Science and Interline Therapeutics. The Chodera laboratory receives or has received funding from multiple sources, including the National Institutes of Health, the National Science Foundation, the Parker Institute for Cancer Immunotherapy, Relay Therapeutics, Entasis Therapeutics, Silicon Therapeutics, EMD Serono (Merck KGaA), AstraZeneca, Vir Biotechnology, Bayer, XtalPi, Interline Therapeutics, the Molecular Sciences Software Institute, the Starr Cancer Consortium, the Open Force Field Consortium, Cycle for Survival, a Louis V. Gerstner Young Investigator Award, and the Sloan Kettering Institute. A complete funding history for the Chodera lab can be found at <http://choderelab.org/funding>. Y.W. has limited financial interests in Flagship Pioneering, Inc.

8 Acknowledgements

The authors thank OpenEye Scientific Software for providing a free academic license to the OpenEye Toolkits. Y.W. acknowledges support from the Schmidt Science Fellowship, in partnership with the Rhodes Trust, and the Simons Center for Computational Physical Chemistry at New York University. J.D.C. acknowledges support from NIH grant P30 CA008748, NIH grant R01 GM132386, NIH grant R01 GM121505, and the Sloan Kettering Institute.

References

- [1] (2020). Openff sandbox gen2 optimization dataset.
- [2] (2020). Pepconf dataset.
- [3] Battaglia, P. W., Hamrick, J. B., Bapst, V., Sanchez-Gonzalez, A., Zambaldi, V., Malinowski, M., Tacchetti, A., Raposo, D., Santoro, A., Faulkner, R., et al. (2018). Relational inductive biases, deep learning, and graph networks. *arXiv preprint arXiv:1806.01261*.
- [4] Behara, P. K., Gokey, T., Cavender, C., Horton, J., Wang, L., Jang, H., Wagner, J., Cole, D., Bayly, C., and Mobley, D. (2023). [openforcefield/openff-forcefields](https://github.com/openforcefield/openff-forcefields).
- [5] Bender, B. J., Gahbauer, S., Luttens, A., Lyu, J., Webb, C. M., Stein, R. M., Fink, E. A., Balias, T. E., Carlsson, J., Irwin, J. J., et al. (2021). A practical guide to large-scale docking. *Nature protocols*, 16(10):4799–4832.
- [6] Boothroyd, S., Behara, P. K., Madin, O., Hahn, D., Jang, H., Gapsys, V., Wagner, J., Horton, J., Dotson, D., Thompson, M., et al. (2022). Development and benchmarking of open force field 2.0.0—the sage small molecule force field.
- [7] Boothroyd, S., Behara, P. K., Madin, O. C., Hahn, D. F., Jang, H., Gapsys, V., Wagner, J. R., Horton, J. T., Dotson, D. L., Thompson, M. W., et al. (2023). Development and benchmarking of open force field 2.0.0: The Sage small molecule force field. *Journal of Chemical Theory and Computation*.
- [8] Case, D., Aktulga, H., Belfon, K., Ben-Shalom, I., Berryman, J., Brozell, S., Cerutti, D., Cheatham, T., III, Cisneros, G., Cruzeiro, V., Darden, T., Forouzesh, N., Giambasu, G., Giese, T., Gilson, M., Gohlke, H., Goetz, A., Harris, J., Izadi, S., Izmailov, S., Kasavajhala, K., Kaymak, M., King, E., Kovalenko, A., Kurtzman, T., Lee, T., Li, P., Lin, C., Liu, J., Luchko, T., Luo, R., Machado, M., Man, V., Manathunga, M., Merz, K., Miao, Y., Mikhailovskii, O., Monard, G., Nguyen, H., O’Hearn, K., Onufriev, A., Pan, F., Pantano, S., Qi, R., Rahnamoun, A., Roe, D., Roitberg, A., Sagui, C., Schott-Verdugo, S., Shajan, A., Shen, J., Simmerling, C., Skrynnikov, N., Smith, J., Swails, J., Walker, R., Wang, J., Wang, J., Wei, H., Wu, X., Wu, Y., Xiong, Y., Xue, Y., York, D., Zhao, S., Zhu, Q., and (2023). Amber 2023.
- [9] Cavender, C. E., Behara, P. K., Boothroyd, S., Dotson, D. L., Horton, J. T., Mitchell, J. A., Pulido, I. J., Thompson, M. W., Wagner, J., Wang, L., Chodera, J. D., Cole, D. J., Mobley, D. L., Shirts, M. R., and Gilson, M. K. (2023). Development and benchmarking of an open, self-consistent force field for proteins and small molecules from the Open Force Field Initiative. Funding from National Institutes of Health grant GM132386.
- [10] Chodera, J., Rizzi, A., Naden, L., Beauchamp, K., Grinaway, P., Fass, J., Wade, A., Rustenburg, B., Ross, G. A., Krämer, A., Macdonald, H. B., Rodríguez-Guerra, J., dominicrufa, Simonett, A., Swenson, D. W. H., hb0402, Henry, M., Roet, S., and Silveira, A. (2021). Choderelab/openmmtools: 0.20.3 Bugfix Release. Zenodo.
- [11] Chodera, J., Wiewiora, R., Stern, C., and peastman (2020). openmm/openmm-forcefields: Fix GAFF AM1-BCC charging bug for some molecules.

[12] Chodera, J. D. and Shirts, M. R. (2011). Replica exchange and expanded ensemble simulations as gibbs sampling: Simple improvements for enhanced mixing. *The Journal of chemical physics*, 135(19):194110.

[13] Coimbatore Narayanan, B., Westbrook, J., Ghosh, S., Petrov, A. I., Sweeney, B., Zirbel, C. L., Leontis, N. B., and Berman, H. M. (2014). The nucleic acid database: new features and capabilities. *Nucleic acids research*, 42(D1):D114–D122.

[14] Coutsias, E. A., Lexa, K. W., Wester, M. J., Pollock, S. N., and Jacobson, M. P. (2016). Exhaustive conformational sampling of complex fused ring macrocycles using inverse kinematics. *Journal of chemical theory and computation*, 12(9):4674–4687.

[15] Dauber-Osguthorpe, P. and Hagler, A. T. (2019). Biomolecular force fields: where have we been, where are we now, where do we need to go and how do we get there? *Journal of computer-aided molecular design*, 33(2):133–203.

[16] Davies, T. G., Bentley, J., Arris, C. E., Boyle, F. T., Curtin, N. J., Endicott, J. A., Gibson, A. E., Golding, B. T., Griffin, R. J., Hardcastle, I. R., et al. (2002). Structure-based design of a potent purine-based cyclin-dependent kinase inhibitor. *Nature structural biology*, 9(10):745–749.

[17] DeMarco, M. L. and Woods, R. J. (2009). Atomic-resolution conformational analysis of the gm3 ganglioside in a lipid bilayer and its implications for ganglioside–protein recognition at membrane surfaces. *Glycobiology*, 19(4):344–355.

[18] DeMarco, M. L., Woods, R. J., Prestegard, J. H., and Tian, F. (2010). Presentation of membrane-anchored glycosphingolipids determined from molecular dynamics simulations and nmr paramagnetic relaxation rate enhancement. *Journal of the American Chemical Society*, 132(4):1334–1338.

[19] Donchev, A. G., Taube, A. G., Decolvenaere, E., Hargus, C., McGibbon, R. T., Law, K.-H., Gregersen, B. A., Li, J.-L., Palmo, K., Siva, K., et al. (2021a). Quantum chemical benchmark databases of gold-standard dimer interaction energies. *Scientific data*, 8(1):55.

[20] Donchev, A. G., Taube, A. G., Decolvenaere, E., Hargus, C., McGibbon, R. T., Law, K.-H., Gregersen, B. A., Li, J.-L., Palmo, K., Siva, K., et al. (2021b). Quantum chemical benchmark databases of gold-standard dimer interaction energies. *Scientific data*, 8(1):55.

[21] Du, J., Zhang, S., Wu, G., Moura, J. M. F., and Kar, S. (2018). Topology Adaptive Graph Convolutional Networks. *arXiv:1710.10370 [cs, stat]*.

[22] Duvenaud, D. K., Maclaurin, D., Iparraguirre, J., Bombarell, R., Hirzel, T., Aspuru-Guzik, A., and Adams, R. P. (2015). Convolutional networks on graphs for learning molecular fingerprints. In *Advances in neural information processing systems*, pages 2224–2232.

[23] Eastman, P., Behara, P. K., Dotson, D. L., Galvelis, R., Herr, J. E., Horton, J. T., Mao, Y., Chodera, J. D., Pritchard, B. P., Wang, Y., et al. (2023). Spice, a dataset of drug-like molecules and peptides for training machine learning potentials. *Scientific Data*, 10(1):11.

[24] Eastman, P., Swails, J., Chodera, J. D., McGibbon, R. T., Zhao, Y., Beauchamp, K. A., Wang, L.-P., Simmonett, A. C., Harrigan, M. P., Stern, C. D., et al. (2017). Openmm 7: Rapid development of high performance algorithms for molecular dynamics. *PLoS computational biology*, 13(7):e1005659.

[25] Friberg, A., Vigil, D., Zhao, B., Daniels, R. N., Burke, J. P., Garcia-Barrantes, P. M., Camper, D., Chauder, B. A., Lee, T., Olejniczak, E. T., et al. (2013). Discovery of potent myeloid cell leukemia 1 (mcl-1) inhibitors using fragment-based methods and structure-based design. *Journal of medicinal chemistry*, 56(1):15–30.

[26] Gilmer, J., Schoenholz, S. S., Riley, P. F., Vinyals, O., and Dahl, G. E. (2017). Neural message passing for quantum chemistry. In *International conference on machine learning*, pages 1263–1272. PMLR.

[27] Gilson, M. K., Gilson, H. S., and Potter, M. J. (2003). Fast assignment of accurate partial atomic charges: an electronegativity equalization method that accounts for alternate resonance forms. *Journal of chemical information and computer sciences*, 43(6):1982–1997.

[28] Gould, I., Skjevik, A., Dickson, C., Madej, B., and Walker, R. (2018). Lipid17: A comprehensive amber force field for the simulation of zwitterionic and anionic lipids. *Manuscript in preparation*.

[29] Hagler, A. T. (2019). Force field development phase ii: Relaxation of physics-based criteria... or inclusion of more rigorous physics into the representation of molecular energetics. *Journal of computer-aided molecular design*, 33(2):205–264.

[30] Hamilton, W., Ying, Z., and Leskovec, J. (2017). Inductive representation learning on large graphs. In *Advances in neural information processing systems*, pages 1024–1034.

[31] Horn, H. W., Swope, W. C., Pitera, J. W., Madura, J. D., Dick, T. J., Hura, G. L., and Head-Gordon, T. (2004). Development of an improved four-site water model for biomolecular simulations: Tip4p-ew. *The Journal of chemical physics*, 120(20):9665–9678.

[32] Horton, J. (2022). openforcefield/openff-qcsubmit: 0.3.1.

[33] Jakalian, A., Bush, B. L., Jack, D. B., and Bayly, C. I. (2000). Fast, efficient generation of high-quality atomic charges. am1-bcc model: I. method. *Journal of computational chemistry*, 21(2):132–146.

[34] Jakalian, A., Jack, D. B., and Bayly, C. I. (2002). Fast, efficient generation of high-quality atomic charges. am1-bcc model: II. parameterization and validation. *Journal of computational chemistry*, 23(16):1623–1641.

[35] Jorgensen, W. L., Chandrasekhar, J., Madura, J. D., Impey, R. W., and Klein, M. L. (1983). Comparison of simple potential functions for simulating liquid water. *The Journal of chemical physics*, 79(2):926–935.

[36] Joung, I. S. and Cheatham III, T. E. (2008). Determination of alkali and halide monovalent ion parameters for use in explicitly solvated biomolecular simulations. *The journal of physical chemistry B*, 112(30):9020–9041.

[37] Joung, I. S. and Cheatham III, T. E. (2009). Molecular dynamics simulations of the dynamic and energetic properties of alkali and halide ions using water-model-specific ion parameters. *The Journal of Physical Chemistry B*, 113(40):13279–13290.

[38] Khouri, G. A., Thompson, J. P., Smadbeck, J., Kieslich, C. A., and Floudas, C. A. (2013). Forcefield_ptm: Ab initio charge and amber forcefield parameters for frequently occurring post-translational modifications. *Journal of chemical theory and computation*, 9(12):5653–5674.

[39] Kim, S., Chen, J., Cheng, T., Gindulyte, A., He, J., He, S., Li, Q., Shoemaker, B. A., Thiessen, P. A., Yu, B., et al. (2023). Pubchem 2023 update. *Nucleic Acids Research*, 51(D1):D1373–D1380.

[40] Kingma, D. P. and Ba, J. (2014). Adam: A method for stochastic optimization. *arXiv preprint arXiv:1412.6980*.

[41] Kipf, T. N. and Welling, M. (2016). Semi-supervised classification with graph convolutional networks. *CoRR*, abs/1609.02907.

[42] Kirschner, K. N., Yongye, A. B., Tschampel, S. M., González-Outeiriño, J., Daniels, C. R., Foley, B. L., and Woods, R. J. (2008). Glycam06: a generalizable biomolecular force field. carbohydrates. *Journal of computational chemistry*, 29(4):622–655.

[43] Labute, P. and Ebert, M. (2021). Optimizing simulations protocols for relative free energy calculations. In *Free Energy Methods in Drug Discovery: Current State and Future Directions*, pages 227–245. ACS Publications.

[44] Landrum, G., Tosco, P., Kelleyand, B., Ric, Cosgrove, D., sriniker, gedeck, Vianello, R., NadineSchneider, Kawashima, E., N, D., Jones, G., Dalke, A., Cole, B., Swain, M., Turk, S., AlexanderSavelyev, Vaucher, A., Wójcikowski, M., Take, I., Probst, D., Ujihara, K., Scalfani, V. F., guillaume godin, Lehtivarjo, J., Pahl, A., Walker, R., Berenger, F., jasonbiggs, and strets123 (2023). rdkit/rdkit: 2023_03_2 (Q1 2023) Release.

[45] Leach, A. R. (2001). *Molecular modelling: principles and applications*. Pearson education.

[46] Leimkuhler, B. and Matthews, C. (2016). Efficient molecular dynamics using geodesic integration and solvent–solute splitting. *Proceedings of the Royal Society A: Mathematical, Physical and Engineering Sciences*, 472(2189):20160138.

[47] Li, P. and Merz Jr, K. M. (2014). Taking into account the ion-induced dipole interaction in the nonbonded model of ions. *Journal of chemical theory and computation*, 10(1):289–297.

[48] Li, P., Roberts, B. P., Chakravorty, D. K., and Merz Jr, K. M. (2013). Rational design of particle mesh ewald compatible lennard-jones parameters for +2 metal cations in explicit solvent. *Journal of chemical theory and computation*, 9(6):2733–2748.

[49] Li, P., Song, L. F., and Merz Jr, K. M. (2015). Parameterization of highly charged metal ions using the 12-6-4 lj-type nonbonded model in explicit water. *The Journal of Physical Chemistry B*, 119(3):883–895.

[50] Li, Q., Cheng, T., Wang, Y., and Bryant, S. H. (2010). Pubchem as a public resource for drug discovery. *Drug discovery today*, 15(23-24):1052–1057.

[51] Liang, J., Tsui, V., Van Abbema, A., Bao, L., Barrett, K., Beresini, M., Berezhkovskiy, L., Blair, W. S., Chang, C., Driscoll, J., et al. (2013). Lead identification of novel and selective tyk2 inhibitors. *European journal of medicinal chemistry*, 67:175–187.

[52] Macdonald, H. B., dfhahn, Henry, M., Chodera, J., Dotson, D., Glass, W., and Pulido, I. (2022). openforcefield/openff-arsenic: v0.2.1.

[53] Maier, J. A., Martinez, C., Kasavajhala, K., Wickstrom, L., Hauser, K. E., and Simmerling, C. (2015). ff14sb: improving the accuracy of protein side chain and backbone parameters from ff99sb. *Journal of chemical theory and computation*, 11(8):3696–3713.

[54] Mey, A. S., Allen, B. K., Macdonald, H. E. B., Chodera, J. D., Hahn, D. F., Kuhn, M., Michel, J., Mobley, D. L., Naden, L. N., Prasad, S., et al. (2020). Best practices for alchemical free energy calculations [article v1. 0]. *Living journal of computational molecular science*, 2(1).

[55] Mobley, D. L., Bannan, C. C., Rizzi, A., Bayly, C. I., Chodera, J. D., Lim, V. T., Lim, N. M., Beauchamp, K. A., Shirts, M. R., Gilson, M. K., et al. (2018a). Open force field consortium: Escaping atom types using direct chemical perception with smirnoff v0. 1. *BioRxiv*, page 286542.

[56] Mobley, D. L., Bannan, C. C., Rizzi, A., Bayly, C. I., Chodera, J. D., Lim, V. T., Lim, N. M., Beauchamp, K. A., Slochower, D. R., Shirts, M. R., et al. (2018b). Escaping atom types in force fields using direct chemical perception. *Journal of chemical theory and computation*, 14(11):6076–6092.

[57] Murphy, R. L., Srinivasan, B., Rao, V. A., and Ribeiro, B. (2018). Janossy pooling: Learning deep permutation-invariant functions for variable-size inputs. *CoRR*, abs/1811.01900.

[58] Parlea, L. G., Sweeney, B. A., Hosseini-Asanjan, M., Zirbel, C. L., and Leontis, N. B. (2016). The rna 3d motif atlas: Computational methods for extraction, organization and evaluation of rna motifs. *Methods*, 103:99–119.

[59] Paszke, A., Gross, S., Massa, F., Lerer, A., Bradbury, J., Chanan, G., Killeen, T., Lin, Z., Gimelshein, N., Antiga, L., Desmaison, A., Kopf, A., Yang, E., DeVito, Z., Raison, M., Tejani, A., Chilamkurthy, S., Steiner, B., Fang, L., Bai, J., and Chintala, S. (2019). Pytorch: An imperative style, high-performance deep learning library. In Wallach, H., Larochelle, H., Beygelzimer, A., d'Alché-Buc, F., Fox, E., and Garnett, R., editors, *Advances in Neural Information Processing Systems 32*, pages 8024–8035. Curran Associates, Inc.

[60] Pérez, A., Marchán, I., Svozil, D., Sponer, J., Cheatham III, T. E., Laughton, C. A., and Orozco, M. (2007). Refinement of the amber force field for nucleic acids: improving the description of α/γ conformers. *Biophysical journal*, 92(11):3817–3829.

[61] Prasad, S., Mobley, D., Braun, E., Mayes, H., Monroe, J., Zuckerman, D., et al. (2018). Best practices for foundations in molecular simulations [article v1. 0]. *Living Journal of Computational Molecular Science*, 1:1–28.

[62] Prasad, V. K., Otero-de La-Roza, A., and DiLabio, G. A. (2019). Pepconf, a diverse data set of peptide conformational energies. *Scientific data*, 6(1):1–9.

[63] Qiu, Y., Smith, D. G., Boothroyd, S., Jang, H., Hahn, D. F., Wagner, J., Bannan, C. C., Gokey, T., Lim, V. T., Stern, C. D., et al. (2021). Development and benchmarking of open force field v1.0.0—the Parsley small-molecule force field. *Journal of chemical theory and computation*, 17(10):6262–6280.

[64] RDKit, online (2013). RDKit: Open-source cheminformatics. <http://www.rdkit.org>. [Online; accessed 11-April-2013].

[65] Rufa, D. A., Zhang, I., Bruce Macdonald, H. E., Grinaway, P. B., Pulido, I., Henry, M. M., Rodríguez-Guerra, J., Wittmann, M., Albanese, S. K., Glass, W. G., Silveira, A., Schaller, D., Naden, L. N., and Chodera, J. D. (2022). Perses. Please cite this software using these metadata.

[66] Schlick, T. (2010). *Molecular modeling and simulation: an interdisciplinary guide*, volume 2. Springer.

[67] Shirts, M. R. and Chodera, J. D. (2008). Statistically optimal analysis of samples from multiple equilibrium states. *The Journal of chemical physics*, 129(12):124105.

[68] Smith, D. G., Altarawy, D., Burns, L. A., Welborn, M., Naden, L. N., Ward, L., Ellis, S., Pritchard, B. P., and Crawford, T. D. (2021). The molssi qcarchive project: An open-source platform to compute, organize, and share quantum chemistry data. *Wiley Interdisciplinary Reviews: Computational Molecular Science*, 11(2):e1491.

[69] Smith, D. G., Burns, L. A., Simmonett, A. C., Parrish, R. M., Schieber, M. C., Galvelis, R., Kraus, P., Kruse, H., Di Remigio, R., Alenaizan, A., et al. (2020). Psi4 1.4: Open-source software for high-throughput quantum chemistry. *The Journal of chemical physics*, 152(18).

[70] Tan, D., Piana, S., Dirks, R. M., and Shaw, D. E. (2018). Rna force field with accuracy comparable to state-of-the-art protein force fields. *Proceedings of the National Academy of Sciences*, 115(7):E1346–E1355.

[71] Tse, C. H., Comer, J., Sang Chu, S. K., Wang, Y., and Chipot, C. (2019). Affordable membrane permeability calculations: permeation of short-chain alcohols through pure-lipid bilayers and a mammalian cell membrane. *Journal of Chemical Theory and Computation*, 15(5):2913–2924.

[72] Wang, J., Wang, W., Kollman, P. A., and Case, D. A. (2006). Automatic atom type and bond type perception in molecular mechanical calculations. *Journal of molecular graphics and modelling*, 25(2):247–260.

[73] Wang, J., Wolf, R. M., Caldwell, J. W., Kollman, P. A., and Case, D. A. (2004). Development and testing of a general amber force field. *Journal of computational chemistry*, 25(9):1157–1174.

[74] Wang, M., Zheng, D., Ye, Z., Gan, Q., Li, M., Song, X., Zhou, J., Ma, C., Yu, L., Gai, Y., et al. (2019a). Deep graph library: A graph-centric, highly-performant package for graph neural networks. *arXiv preprint arXiv:1909.01315*.

[75] Wang, Y., Fass, J., Kaminow, B., Herr, J. E., Rufa, D., Zhang, I., Pulido, I., Henry, M., Bruce Macdonald, H. E., Takaba, K., and Chodera, J. D. (2022). End-to-end differentiable construction of molecular mechanics force fields. *Chem. Sci.*, 13:12016–12033.

[76] Wang, Y., Fass, J., Stern, C. D., Luo, K., and Chodera, J. (2019b). Graph nets for partial charge prediction. *arXiv preprint arXiv:1909.07903*.

[77] Wang, Y., Pulido, I., Takaba, K., Kaminow, B., Scheen, J., Wang, L., and Chodera, J. D. (2023). Espalomacharge: Machine learning-enabled ultra-fast partial charge assignment. *arXiv preprint arXiv:2302.06758*.

[78] Wang, Y., Sun, Y., Liu, Z., Sarma, S. E., Bronstein, M. M., and Solomon, J. M. (2019c). Dynamic graph cnn for learning on point clouds. *AcM Transactions On Graphics (tog)*, 38(5):1–12.

[79] Wu, F., Zhang, T., Souza Jr, A. H. d., Fifty, C., Yu, T., and Weinberger, K. Q. (2019). Simplifying graph convolutional networks. *arXiv preprint arXiv:1902.07153*.

[80] Xu, H. (2019). Optimal measurement network of pairwise differences. *Journal of Chemical Information and Modeling*, 59(11):4720–4728.

[81] Xu, K., Hu, W., Leskovec, J., and Jegelka, S. (2018). How powerful are graph neural networks? *arXiv preprint arXiv:1810.00826*.

[82] Zgarbová, M., Sponer, J., Otyepka, M., Cheatham III, T. E., Galindo-Murillo, R., and Jurecka, P. (2015). Refinement of the sugar-phosphate backbone torsion beta for amber force fields improves the description of z-and b-dna. *Journal of chemical theory and computation*, 11(12):5723–5736.

Appendix: Espaloma-0.3.0: Machine-learned molecular mechanics force field for the simulation of protein-ligand systems and beyond.

Kenichiro Takaba (ORCID: [0000-0002-2481-8830](#))^{1, 2}, Iván Pulido (ORCID: [0000-0002-7178-8136](#))¹,
Mike Henry (ORCID: [0000-0002-3870-9993](#))¹, Hugo MacDermott-Opeskin (ORCID: [0000-0002-7393-7457](#))¹,
John D. Chodera (ORCID: [0000-0003-0542-119X](#))¹,
Yuanqing Wang² (ORCID: [0000-0003-4403-2015](#))^{3, 1}

¹Computational and Systems Biology Program, Sloan Kettering Institute, Memorial Sloan Kettering Cancer Center, New York, N.Y. 10065; ²Pharmaceutical Research Center, Advanced Drug Discovery, Asahi Kasei Pharma Corporation, Shizuoka 410-2321, Japan; ³New York University, New York, N.Y. 10004

*For correspondence:
john.chodera@choderlab.org (JDC); wangyq@wangyq.net (YW)

A Code availability

The data and Python code used to produce the results discussed in this paper is distributed open-source under an MIT license and is available at <https://github.com/choderlab/espaloma-0.3.0-manuscript>.

Core dependencies include a modified version of Espaloma 0.3.0 release [75] (<https://github.com/choderlab/espaloma/tree/4c6155b72d00ce0190b3cb551e7e59f0adc33a56>), PyTorch 1.1.2 [59], Deep Graph Library 0.9.0 [76], and Open Force Field Toolkit 0.10.6 [55], to refit and evaluate the espaloma model. A modified version of Openmmforcefields 0.11.0 [11] (<https://github.com/kntkb/openmmforcefields/tree/6d2c3cd33d9800a32032d28b6b2dca92f348a43>) was used to run all the relative alchemical protein-ligand binding free energy calculations with Perses 0.10.1 infrastructure [65]. Espaloma 0.2.4 release and a modified version of Espaloma 0.3.0 was used to parametrize small molecules with espaloma-0.2.2 and espaloma-0.3.0, respectively. A modified version of Perses 0.10.1 (<https://github.com/kntkb/perses/tree/0d069fc1cf31b8cce1a> [e7a1482c3fa46bc1382d2](https://github.com/kntkb/perses/tree/e7a1482c3fa46bc1382d2)) was used to self-consistently parametrize both small molecules and proteins with espaloma-0.3.0. A modified version of cinnabar 0.3.0 [52] (<https://github.com/kntkb/cinnabar/tree/de7bc6623fb25d75848aa1c9f538b77cd02a4b01>) was used to support arbitrary tick frequency when plotting ΔG and $\Delta\Delta G$ plots.

B MolSSI QCArchive QM datasets

The Python code used to download the quantum mechanics (QM) datasets from the MolSSI QCArchive [32] is available at <https://github.com/choderlab/download-qca-datasets>. The QM datasets utilized in this study were obtained from various workflows implemented in the QCArchive ecosystem, including Dataset, OptimizationDataset, and TorsionDriveDataset generated at the B3LYP-D3BJ/DZVP level of theory. This level of theory was chosen to maintain consistency with the Open Force Field initiative [63], and it is expected to balance computational efficiency and accuracy in reproducing conformations generated by higher-level theories.

The QM datasets in Table 1 are composed of the following datasets deposited in QCArhive and annotated based on their respective categories.

²Work partly done while at Memorial Sloan Kettering Cancer Center.

Small molecules

- **SPICE-Pubchem**^{3 4 5 6 7 8} is a collection of Dataset that contains a comprehensive and diverse collection of small, drug-like molecules obtained from Pubchem. It includes atoms within the range of 3 to 50, including hydrogens, and encompasses the elements of Br, C, Cl, F, H, I, N, O, P, and S.
- **SPICE-DES-Monomers**⁹ is a Dataset, sourced from DES370K [20], consists of small molecules (up to 22 atoms) chosen to cover a wide range of chemical space, including the elements of Br, C, Cl, F, H, I, N, O, P, and S.
- **Gen2-Opt**^{10 11 12 13 14} is a collection of OptimizationDataset that contains drug-like molecules used for the parametrization of the OpenFF 1.2.0 ("Parsley") [63] small molecule force field developed by the Open Force Field Consortium. This dataset is part of the datasets used to generate the first generation espaloma force field, espaloma-0.2.2.
- **Gen2-Torsion**^{15 16 17 18 19 20 21 22 23 24 25 26} is a collection TorsionDriveDataset that contains torsion scans of drug-like molecules which is part of the dataset used for the parameterization of the OpenFF 2.0.0 ("Sage") [7] small molecule force field developed by the Open Force Field Consortium.

³Source: <https://github.com/openforcefield/qca-dataset-submission/tree/master/submissions/2021-11-08-QMDataset-pubchem-set1-single-points>

⁴Source: <https://github.com/openforcefield/qca-dataset-submission/tree/master/submissions/2021-11-08-QMDataset-pubchem-set2-single-points>

⁵Source: <https://github.com/openforcefield/qca-dataset-submission/tree/master/submissions/2021-11-09-QMDataset-pubchem-set3-single-points>

⁶Source: <https://github.com/openforcefield/qca-dataset-submission/tree/master/submissions/2021-11-09-QMDataset-pubchem-set4-single-points>

⁷Source: <https://github.com/openforcefield/qca-dataset-submission/tree/master/submissions/2021-11-09-QMDataset-pubchem-set5-single-points>

⁸Source: <https://github.com/openforcefield/qca-dataset-submission/tree/master/submissions/2021-11-09-QMDataset-pubchem-set6-single-points>

⁹Source: <https://github.com/openforcefield/qca-dataset-submission/tree/master/submissions/2021-11-15-QMDataset-DES-monomers-single-points>

¹⁰Source: <https://github.com/openforcefield/qca-dataset-submission/tree/master/submissions/2020-03-20-OpenFF-Gen-2-Optimization-Set-1-Roche>

¹¹Source: <https://github.com/openforcefield/qca-dataset-submission/tree/master/submissions/2020-03-20-OpenFF-Gen-2-Optimization-Set-2-Coverage>

¹²Source: <https://github.com/openforcefield/qca-dataset-submission/tree/master/submissions/2020-03-20-OpenFF-Gen-2-Optimization-Set-3-Pfizer-Discrepancy>

¹³Source: <https://github.com/openforcefield/qca-dataset-submission/tree/master/submissions/2020-03-20-OpenFF-Gen-2-Optimization-Set-4-eMolecules-Discrepancy>

¹⁴Source: <https://github.com/openforcefield/qca-dataset-submission/tree/master/submissions/2020-03-20-OpenFF-Gen-2-Optimization-Set-5-Bayer>

¹⁵Source: <https://github.com/openforcefield/qca-dataset-submission/tree/master/submissions/2020-03-12-OpenFF-Gen-2-Torsion-Set-1-Roche>

¹⁶Source: <https://github.com/openforcefield/qca-dataset-submission/tree/master/submissions/2020-03-23-OpenFF-Gen-2-Torsion-Set-1-Roche-2>

¹⁷Source: <https://github.com/openforcefield/qca-dataset-submission/tree/master/submissions/2020-03-12-OpenFF-Gen-2-Torsion-Set-2-Coverage>

¹⁸Source: <https://github.com/openforcefield/qca-dataset-submission/tree/master/submissions/2020-03-23-OpenFF-Gen-2-Torsion-Set-2-Coverage-2>

¹⁹Source: <https://github.com/openforcefield/qca-dataset-submission/tree/master/submissions/2020-03-12-OpenFF-Gen-2-Torsion-Set-3-Pfizer-Discrepancy>

²⁰Source: <https://github.com/openforcefield/qca-dataset-submission/tree/master/submissions/2020-03-23-OpenFF-Gen-2-Torsion-Set-3-Pfizer-Discrepancy-2>

²¹Source: <https://github.com/openforcefield/qca-dataset-submission/tree/master/submissions/2020-03-12-OpenFF-Gen-2-Torsion-Set-4-eMolecules-Discrepancy>

²²Source: <https://github.com/openforcefield/qca-dataset-submission/tree/master/submissions/2020-03-23-OpenFF-Gen-2-Torsion-Set-4-eMolecules-Discrepancy-2>

²³Source: <https://github.com/openforcefield/qca-dataset-submission/tree/master/submissions/2020-03-12-OpenFF-Gen-2-Torsion-Set-5-Bayer>

²⁴Source: <https://github.com/openforcefield/qca-dataset-submission/tree/master/submissions/2020-03-26-OpenFF-Gen-2-Torsion-Set-5-Bayer-2>

²⁵Source: <https://github.com/openforcefield/qca-dataset-submission/tree/master/submissions/2020-03-12-OpenFF-Gen-2-Torsion-Set-6-supplemental>

²⁶Source: <https://github.com/openforcefield/qca-dataset-submission/tree/master/submissions/2020-03-26-OpenFF-Gen-2-Torsion-Set-6-supplemental-2>

Peptides

- **SPICE-Dipeptide**²⁷ is a Dataset that contains a broad coverage of the possible dipeptides capped with ACE and NME groups formed by the 20 natural amino acids and their common protonation variants. This includes two forms of CYS (neutral or negatively charged), two forms of GLU (neutral or negatively charged), two forms of ASP (neutral or negatively charged), two forms of LYS (neutral or positively charged), and three forms of HIS (neutral forms with a hydrogen on either ND1 or NE2, and a positively charged form with hydrogens on both).
- **Pepconf-Opt**²⁸ is a OptimizationDataset that contains short peptides, including capped, cyclic, and disulfide-bonded peptides originally sourced from Prasad et al. [62] and regenerated by the Open Force Field Consortium. In this study, the `default-dlc` QC specification was utilized, differing from the one used in the first generation espaloma force field (`espaloma-0.2.2`) [75], leading to improved self-consistent field convergence.
- **Protein-torsion**^{29 30 31 32} is a collection of TorsionDriveDataset that contains various torsion scans of polypeptides generated by the Open Force Field Consortium for the OpenFF 3.x ("Rosemary") force field [9]. These torsion scans cover χ_1 and χ_2 angles in the rotatable side chains, as well as ϕ , ψ , and ω angles in the backbones.

RNA

- **RNA-Diverse**³³ is a Dataset that contains comprehensive and diverse collection of experimental RNA structures. It includes 138 base pair structures and 295 base triple structures sourced from the Nucleic Acid Database [13]. Additionally, the dataset contains 4,056 representative trinucleotide structures obtained from the RNA Structure Atlas website [58], where the experimentally observed internal and hairpin loop motifs, as well as junction loops of representative sets of RNA 3D Structures with an X-ray resolution cutoff of 2.5 Å, were segmented into all possible trinucleotide permutations, resulting in 64 unique molecules. These trinucleotide structures are capped with O5' hydroxyl groups at the 5' end and clustered to select the representative structures. For the espaloma refitting experiment, only the trinucleotides were utilized.
- **RNA-Trinucleotide**³⁴ is a Dataset that provides a broader and more diverse structural coverage of trinucleotides compared to the **RNA-Diverse** dataset.
- **RNA-Nucleoside**³⁵ is a Dataset that comprises a comprehensive and diverse collection of nucleosides (adenosine, guanosine, cytidine, and uridine) without O5' hydroxyl atoms. These nucleosides are generated using 500K implicit solvent MD and torsion scanning on N-glycosidic bond (χ torsion) that connects the base and sugar, resulting in diverse sugar pucker conformations and extensive coverage of χ torsions.

C Espaloma refitting experiment

The Python code used to refit and evaluate `espaloma-0.3.0` is available at <https://github.com/choderala/b/refit-espaloma>. It should be noted that `espaloma-0.3.0` is no longer compatible with `espaloma-0.2.x` models and vice versa.

²⁷Source: <https://github.com/openforcefield/qca-dataset-submission/tree/master/submissions/2021-11-08-QMDataset-Dipeptide-single-points>

²⁸Source: <https://github.com/openforcefield/qca-dataset-submission/tree/master/submissions/2020-10-26-PEPCONF-Optimization>

²⁹Source: <https://github.com/openforcefield/qca-dataset-submission/tree/master/submissions/2021-11-18-OpenFF-Protein-Dipeptide-2D-TorsionDrive>

³⁰Source: <https://github.com/openforcefield/qca-dataset-submission/tree/master/submissions/2022-02-10-OpenFF-Protein-Capped-1-mer-Sidechains>

³¹Source: <https://github.com/openforcefield/qca-dataset-submission/tree/master/submissions/2022-05-30-OpenFF-Protein-Capped-3-mer-Backbones>

³²Source: <https://github.com/openforcefield/qca-dataset-submission/tree/master/submissions/2023-02-06-OpenFF-Protein-Capped-3-mer-Omega>

³³Source: <https://github.com/openforcefield/qca-dataset-submission/tree/master/submissions/2022-07-07-RNA-basepair-triplebase-single-points>

³⁴Source: <https://github.com/openforcefield/qca-dataset-submission/tree/master/submissions/2022-10-21-RNA-trinucleotide-single-points>

³⁵Source: <https://github.com/openforcefield/qca-dataset-submission/tree/master/submissions/2023-03-09-RNA-nucleoside-single-points>

C.1 Data preparation

The QM datasets obtained from the QC Archive [68] in **SI Section B** were preprocessed prior to the refitting experiment. Molecules with a gap between the minimum and maximum energy larger than 0.1 Hartree (62.5 kcal/mol) were excluded. Since the van der Waals parameters affect the physical property prediction, which is computationally challenging to optimize, we focus on optimizing the valence parameters and use openff-2.0.0 force field [7] for the van der Waals parameters. AM1BCC-ELF10 partial charges were pre-computed using the OpenEye toolkit as reference charges. These charges were then used to predict the atomic partial charges based on the predicted electronegativity and hardness of atoms, following the same protocol described in the earlier works by Wang et al. [75]. To ensure that each molecule was represented only once, duplicate molecules across different datasets were merged, ensuring that unique molecules were distributed among the train, validate, or test dataset.

C.2 Machine learning experimental details

C.2.1 Input features

One of the improvements made from the previous espaloma model [75] is the exclusion of resonance-sensitive features, such as valences and formal charges, in order to improve the handling of molecules with atomic resonance, such as guanidinium and carboxylic acid. In this study, the input features of the atoms included the one-hot encoded element, as well as the hybridization, aromaticity, ring membership of sizes 3 to 8, atom mass, and the degree of the atoms, which is defined as the number of directly-bonded neighbors, all assigned using the RDKit 2023-03-4 release package [44].

C.2.2 Hyperparameter optimization

The hyperparameters were briefly optimized utilizing a subset of data from **SI Section B**, which included OpenFF Gen2-Opt, SPICE-Dipeptide, and RNA-Diverse datasets. The data was partitioned into train : validate : test sets in a 40 : 30 : 30 ratio. During the training process, energy and force matching were applied, along with partial charge fitting using the charge equilibrium approach, as in [75, 77].

$$\mathcal{L} = W_{\text{energy}} \mathcal{L}_{\text{energy}} + W_{\text{force}} \mathcal{L}_{\text{force}} + W_{\text{charge}} \mathcal{L}_{\text{charge}} \quad (2)$$

Following the protocol specified in Wang et al. [75], we utilized GraphSAGE [30] as the graph neural network model, the Adam optimizer [40], and the Rectified Linear Unit (ReLU) activation function, while maintaining the energy and charge loss weights to 1 and 1e-3, respectively, throughout the optimization experiment. The hyperparameters subject to optimization included the batch size (32, 64, 128, 256), the depth of the graph neural network (2, 3, 4, 5), the depth of the Janossy pooling network (2, 3, 4, 5), the learning rates (1e-3, 1e-4, 5e-5, 1e-5), the number of units per layer (64, 128, 256, 512), and the force weights (1, 1e-1, 1e-2, 1e-3, 1e-4) via grid search on the validation set, and trained for 3000 epochs for each optimization experiment.

As a result, the optimal configuration was determined as follows: For the atom embedding stage (Stage1), three GraphSAGE layers with 512 units and ReLU activation function were employed. For the symmetry preserving pooling stage (Stage2) and the readout stage (Stage3), four feed-forward layers with 512 units and ReLU activation, a learning rate of 1e-4, and a force loss weight of 1.

C.2.3 Production run

The datasets from **SI Section B** were partitioned into train, validate, and test sets with a distribution of 80:10:10 ratio, respectively, with few exceptions. Notably, the entire RNA-Nucleoside dataset was exclusively utilized for the train set, while the entire RNA-Trinucleoside dataset was allocated for the test set. This partitioning scheme was designed to incorporate diverse molecular structures and enable a comprehensive evaluation of the performance of the espaloma model.

It should be noted that the espaloma model, trained with the hyperparameters described above, reproduced poor torsion profiles, which led to out-of-plane geometries after molecular minimization using the trained espaloma model. We found that this problem could be remedied by truncating the improper torsion

terms to only $n = 1, 2$ periodicities, instead of $n = 1, \dots, 6$ as in the original method [75], and by utilizing regularization for the proper and improper torsion force constants. Additionally, we discovered that increasing the loss weight on the charge term improved the prediction of partial charges and better recapitulated the electrostatic potentials.

Regarding these findings, the final espaloma model was trained with the following loss function with all weights set to 1:

$$\mathcal{L} = W_{\text{energy}} * \mathcal{L}_{\text{energy}} + W_{\text{force}} * \mathcal{L}_{\text{force}} + W_{\text{proper}} * \mathcal{L}_{\text{proper}} + W_{\text{improper}} * \mathcal{L}_{\text{improper}} \quad (3)$$

To prevent overfitting and ensure optimal model performance, we applied dropouts to the atom embedding stage (Stage 1) and symmetry-preserving stage (Stage 2), as well as implemented an early stopping mechanism. After 800 epochs, the joint root mean square error (RMSE) loss, which incorporates both energies and forces, was monitored using the validation set. This approach allowed us to identify the point at which further training no longer improved the model's generalization capability.

D Protein-ligand benchmark dataset

The protein-ligand benchmark dataset can be found at <https://github.com/kntkb/protein-ligand-benchmark-custom>. It consists of 4 target systems (Tyk2, Cdk2, P38, and Mcl1) and a total of 76 ligands. This dataset was curated from the openforcefield/protein-ligand-benchmark repository (<https://github.com/openforcefield/protein-ligand-benchmark/tree/d3387602bbeb0167abf00dfb81753d8936775dd2>). The protein structures and ligand poses, as well as the ligand transformations, were manually curated, while the experimental results were adopted from the original repository. The protein and ligand structures were prepared using Maestro from Schrodinger 2022-2.

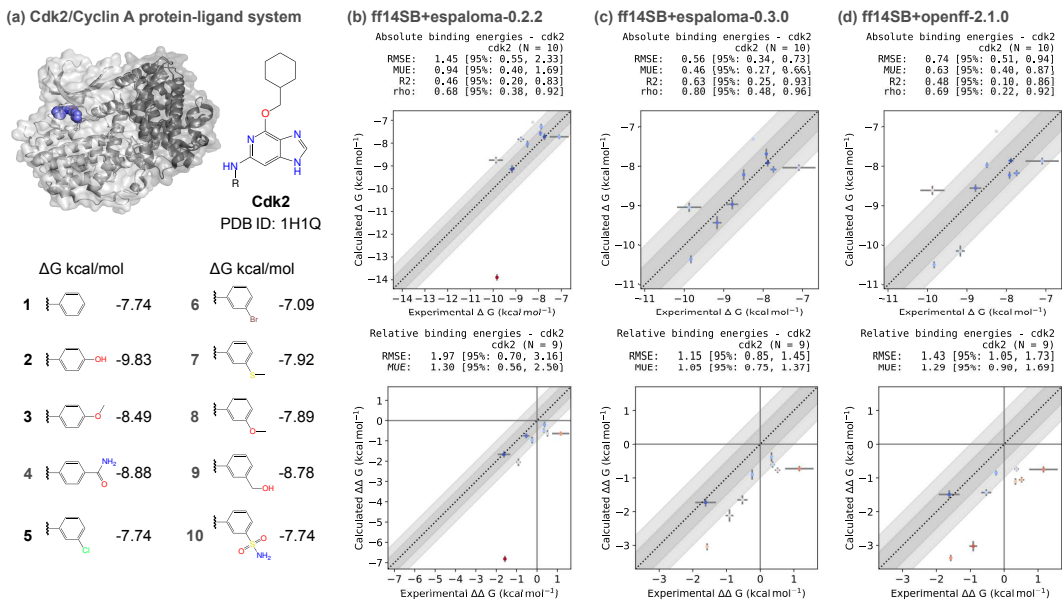
The PDB structure of a protein-ligand complex was imported and processed using the default settings of `prepwizard`, along with additional options including filling in missing side chains and loops using Prime, capping termini, and deleting waters beyond 5.0 Å from het groups. The tautomer states of the ligand complexed with the protein were manually inspected, and the most reasonable state was chosen from a human perspective. For the protein residues, the protonation and tautomer states were optimized using the default settings of `H-bond` assignment. Subsequently, a restrained minimization was performed using the OPLS4 force field, with an RMSD convergence threshold of 0.3 Å for the heavy atoms. The exported protein structure from the complex served as the initial protein structure, and X-ray water molecules were exported if necessary, such as buried water molecules in the binding pocket.

For the ligand poses, a flexible ligand alignment approach was applied with respect to the PDB ligand pose found in the protein-ligand complex structure. The default settings of `ligprep` were used to generate all possible ligand tautomer states, which were then visually inspected to choose the most reasonable state. Subsequently, ligand alignment was performed by aligning all ligands to the PDB ligand pose found in the protein-ligand complex structure, using the `Ligand Alignment` module in Maestro with Bemis-Murcko scaffold or maximum common scaffold constrain. The ligand poses were manually adjusted, taking into account the binding site environment, which involved rotating ligand torsions and minimizing selected atoms to alleviate severe atom clashes and obtain better initial poses.

Finally, the ligand transformation networks were defined manually by human experts, creating a outward radial map with the simplest ligand in the center. In the case of P38 and Mcl1, R-group substituent from multiple scaffold positions and scaffold hopping were observed. In such cases, ligand transformations were grouped into categories to resemble different structure-activity relationship purposes while maintaining a simplified ligand transformation network.

E Alchemical free energy calculations using protein-ligand benchmark dataset

The Python code used to perform the alchemical protein-ligand binding free energy benchmark experiment is available at <https://github.com/choderalab/pl-benchmark-espaloma-experiment>. We utilized the Perses 0.10.1 relative alchemical free energy calculation infrastructure [65], which is based on OpenMM 8.0.0 [24],



Appendix 0 Figure 4. Training espaloma-0.3.0 on an extensive quantum chemical dataset significantly improves protein-ligand binding affinity calculations on the Cdk2 system. (a) We show the X-ray structure used for all free energy calculation as well as the 2D structures of all ligands in the Cdk2 protein-ligand benchmark dataset. An outward radial map with ligand #1 in the center was used for the alchemical ligand transformations. We used the Perses 0.10.1 relative free energy calculation infrastructure [65] to calculate the relative free energy and assess the performance using (b) espaloma-0.2.2 [75], (c) espaloma-0.3.0, and (d) openff-2.1.0 [4]. Amber ff14SB force field [53] used to parametrize the protein for all cases. espaloma-0.2.2 and espaloma-0.3.0 achieves an absolute free energy (ΔG) RMSE of 1.45 [95% CI: 0.55, 2.33] and 0.56 [95% CI: 0.34, 0.73], respectively, indicating that espaloma-0.3.0 trained on extensive quantum chemical dataset significantly improved protein-ligand binding affinity calculations on the Cdk2 system.

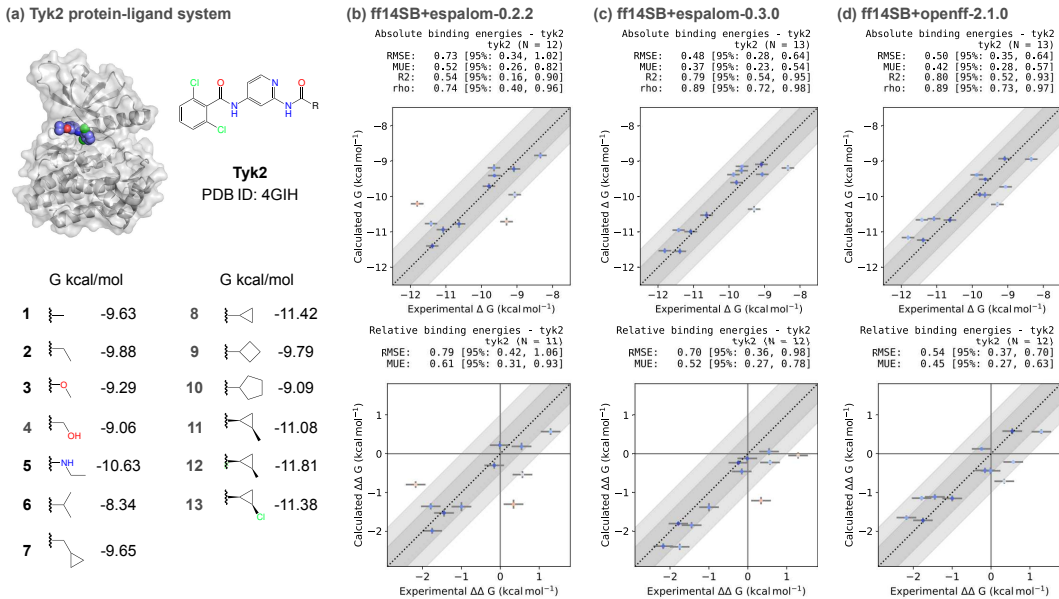
openmmtools 0.22.1 [10], and a modified version of openmmforcefields 0.11.0 package [11] (<https://github.com/kntkb/openmmforcefields/tree/6d2c3dc33d9800a32032d28b6b2dca92f348a43>) to support espaloam-0.3.0.

All systems were solvated with TIP3P water [35] with 9.0 Å buffer around the protein, and the system was neutralized with the Joung and Cheatham monovalent counterions [36] with 300 mM NaCl salt concentration. The protein was parametrized with Amber ff14SB force field [53], and the small molecules were parametrized with openff-2.1.0 [4], espaloma-0.3.0, or espaloma-0.2.2 [75]. Additionally, the protein-ligand was self-consistently parametrized with espaloam-0.3.0, and a modified version of Perses 0.10.1 (<https://github.com/kntkb/perses/tree/0d069fc1cf31b8cce1ae7a1482c3fa46bc1382d2>) was used to perform the protein-ligand binding free energy calculations.

Alchemical free energy calculations were simulated with replica exchange among Hamiltonians with Gibbs sampling [12]. All simulations were performed with 12 alchemical states for 10 ns/replica for Tyk2 and Cdk2, 15 ns/replica for Mcl1, and 20 ns/replica for P38, with replica exchange attempts made every 1 ps. The simulations were performed at 300 K and 1 atm using a Monte Carlo Barostat and Langevin BAOAB integrator [46] with a collision rate of 1/ps. Bonds to hydrogen were constrained, and hydrogen atom masses were set to 3.0 amu by transferring the masses connected to the heavy atoms, allowing for simulations with a 4 fs timestep.

Atom mappings were generated from the provided geometries in the benchmark set. Atoms within 0.5 Å of the transforming ligand pairs were detected as valid mapping atoms using the `use_given_geometries` functionality in Perses.

PyMBAR 3.1.1 [67] was used to compute the relative free energy, while absolute free energies up to an additive constant were estimated using a least-squares estimation strategy [80] using a modified version of OpenFE cinnabar 0.3.0 package [52] (<https://github.com/kntkb/cinnabar/tree/de7bc6623fb25d75848aa1c9f538b77cd02a4b01>). Both experimental and calculated absolute free energies were shifted to their respective means before computing the statistics.



Appendix 0 Figure 5. Training espaloma-0.3.0 on an expanded quantum chemical dataset improves protein-ligand binding affinity on the Tyk2 system. (a) We show the X-ray structure used for all free energy calculation as well as the 2D structures of all ligands in the Tyk2 protein-ligand benchmark dataset. An outward radial map with ligand #1 in the center was used for the alchemical ligand transformations. We used the Perses 0.10.1 relative free energy calculation infrastructure [65] to calculate the relative free energy and assess the performance using (b) espaloma-0.2.2 [75], (c) espaloma-0.3.0, and (d) openff-2.1.0 [4]. Amber ff14SB force field [53] used to parametrize the protein for all cases. Notably, espaloma-0.2.2 failed to simulate the alchemical transformation of ligand #1 to ligand #2; hence one ligand is not reported in (b). espaloma-0.2.2 and espaloma-0.3.0 achieves an absolute free energy (ΔG) RMSE of 0.73 [95% CI: 0.34, 1.02] and 0.48 [95% CI: 0.28, 0.64], respectively, suggesting that espaloma-0.3.0 tends to show improved performance over espaloma-0.2.2.